# Hybrid Precoded Spatial Modulation (hPSM) for mmWave Massive MIMO Systems Over Frequency-Selective Channels

Jinpeng Li<sup>®</sup>, Shijian Gao<sup>®</sup>, Xiang Cheng<sup>®</sup>, Senior Member, IEEE, and Liuqing Yang<sup>®</sup>, Fellow IEEE

Abstract—Precoded spatial modulation (PSM) is well-known for its simple receiver design and superior error performance. To fully inherit its advantages and overcome its unfeasibility to mmWave hybrid massive multi-input multi-output (mMIMO) systems, a novel hybrid PSM (hPSM) is carefully proposed. Except for a similar digital design, hPSM distinctly differs from PSM for its dependence on the analog part of the mmWave mMIMO transceivers. Moreover, unlike PSM where the relevant design suffices to be restricted on a single subcarrier, hPSM requires joint consideration across all subcarriers. Thanks to our judicious design, the error performance of hPSM is optimized and demonstrated to be advantageous over its non-hPSM counterpart. Meanwhile, the overall design is compatible with prevalent hybrid mmWave systems and enjoys a low implementation complexity.

Index Terms—hPSM, mmWave, hybrid massive multi-input multi-output, error performance, analog part.

#### I. INTRODUCTION

N RECENT years, spatial modulation (SM) has been widely studied in multi-input multi-output (MIMO) systems. The main idea of SM is to map the index bits according to the activation status of antennas and symbol bits according to the adopted constellation diagram [1], [2], e.g., phase shift keying (PSK) and quadrature amplitude modulation (QAM). Based on SM, many other variants (e.g., GSM [3], PSM [4], VSM [5], just to name a few) have been proposed and validated with good performance in different applications.

Motivated by the superiority of SM and its extensions, their application to state-of-the-art hybrid mmWave massive MIMO (mMIMO) systems is well anticipated. Unfortunately, a naive transplantation may suffer from severe performance degradation. To be specific, mmWave propagation is well-known

Manuscript received October 17, 2019; revised January 6, 2020; accepted January 30, 2020. Date of publication February 10, 2020; date of current version June 10, 2020. This work was supported in part by the Ministry National Key Research and Development Project under Grant 2017YFE0121400, in part by the Open Research fund of Key Laboratory of Wireless Sensor Network and Communication under Grant 2017003, in part by the Shanghai Institute of Microsystem and Information Technology, Chinese Academy of Sciences, and in part by the National Science Foundation under Grant CPS-1932413 and Grant ECCS-1935915. The associate editor coordinating the review of this article and approving it for publication was Y. Gao. (Corresponding author: Xiang Cheng.)

Jinpeng Li and Xiang Cheng are with the State Key Laboratory of Advanced Optical Communication Systems and Networks, Department of Electronics, School of Electronics Engineering and Computing Sciences, Peking University, Beijing 100080, China, and also with the Key Laboratory of Wireless Sensor Network and Communication, Shanghai Institute of Microsystem and Information Technology, Chinese Academy of Sciences, Shanghai 200050, China (e-mail: jinpenglipku@163.com; xiangcheng@pku.edu.cn).

Shijian Gao and Liuqing Yang are with the Department of Electrical and Computer Engineering, Colorado State University, Fort Collins, CO 80523 USA (e-mail: sjgao@colostate.edu; lqyang@engr.colostate.edu).

Digital Object Identifier 10.1109/LWC.2020.2972866

to exhibit limited scattering [6], leading to highly correlated mMIMO channels. The strong correlation in the spatial domain will impose significant ambiguity on the identification of spatial index patterns, resulting in compromised error performance [7]. Meanwhile, as mmWave channels have ultrawide bandwidth, orthogonal-frequency-division-multiplexing (OFDM) is typically adopted to cope with frequency selectivity [8]. For a hybrid system, however, even though its digital part can be designed independently for each subcarrier, its analog part has to be shared by all subcarriers. Therefore, the resultant index modulation requires joint consideration of all subcarriers, which is drastically different from conventional SM techniques.

Among various SM techniques, in this letter, we hold a particular interest for PSM due to the advantages of lower receiver complexity and better error performance. However, the aforementioned issues imply that direct application of PSM to hybrid mmWave mMIMO is not feasible. Therefore, we judiciously devise a novel PSM-like index modulation (IM) dedicated to hybrid mmWave mMIMO, and term it as hybrid PSM (hPSM). As can be inferred from the name, hPSM includes both the analog part and the digital part. First, by naturally exploiting the analog part of the transceivers, the high-dimension high-correlation spatial channel is converted into the low-dimension and potentially low-correlation "virtual spatial channel" (VSC) encountered from the transmitter radio frequency (RF) chains to receiver RF chains. Second, by utilizing the concept of VSC, the digital precoding is performed with the index mapping incorporated therein. Despite a similar digital part as that of PSM, two striking features make hPSM distinctly different from PSM. First, the VSC where hPSM is implemented is not an actual channel, but a virtual channel determined by the analog part. Second, even with OFDM, all subcarriers still share a common analog part in the hybrid system, making all VSCs intervened. Therefore, hPSM is essentially an IM whose performance is dictated by the design of the analog part. To get an optimized analog part, we derive an approximate expression of the system asymptotic pairwise error probability (APEP), and then devise a low-complexity method to construct the analog part under the target of minimizing APEP. Thanks to our careful treatment, the proposed hPSM could gain remarkable advantages over existing alternatives in terms of the error performance.

Notations: a, a, A represent a scalar, a vector and a matrix, respectively.  $(a)_i$  represents the i-th entry of the vector a.  $(A)_{i,j}$ ,  $(A)_{i,:}$  and  $(A)_{:,j}$  denote the (i,j) entry, the i-th row and the j-th column of A.  $A^T$ ,  $A^*$  and tr(A) represent the transpose, Hermitian transpose and trace of A.

2162-2345 © 2020 IEEE. Personal use is permitted, but republication/redistribution requires IEEE permission. See https://www.ieee.org/publications/rights/index.html for more information.

#### II. SYSTEM AND CHANNEL MODELS

A general hybrid mmWave mMIMO system is considered here, where  $N_t$  antennas with  $N_{RF}^t$  ( $N_{RF}^t \ll N_t$ ) RF chains are deployed at the transmitter, and  $N_r$  antennas with  $N_{RF}^r$  ( $N_{RF}^r \ll N_r$ ) RF chains are deployed at the receiver. The transmitter communicates with the receiver via  $N_s$  data streams, with  $N_s \leq N_{RF}$  and  $N_{RF} = \min\{N_{RF}^t, N_{RF}^r\}$ . Without loss of generality, we further assume  $N_s = N_{RF}$ .

Similar to [9], we adopt a geometric mmWave channel model consisting of  $N_p$  dominant paths and  $N_c$  taps. The tap-d channel,  $\mathbf{H}[d] \in \mathbb{C}^{N_r \times N_t}$ , can be represented by

$$\mathbf{H}[d] = \sum_{l=1}^{N_p} \sqrt{\frac{N_t N_r}{N_p}} \alpha_l p(dT_s - \tau_l) \boldsymbol{a}_r(\phi_l) \boldsymbol{a}_t^*(\theta_l), \ 0 \le d < N_c.$$

For path-l,  $\alpha_l \sim \mathcal{CN}(0,1)$  is the complex gain; p(t) is the pulse-shaping response for  $T_s$ -spaced signaling;  $\tau_l$  is the propagation delay obeying a uniform distribution on  $[0,(N_c-1)T_s]$ ;  $\phi_l$  and  $\theta_l$  are the angle of arrival (AoA) and the angle of departure (AoD), respectively, both uniformly distributed on  $[0,2\pi)$ ;  $a_t(\theta)$  and  $a_r(\phi)$  are the transmitter and receiver array responses, respectively.

With the half-wavelength spaced uniform linear array (ULA) employed at the transceivers, we have  $\boldsymbol{a}_t(\theta) = \frac{1}{\sqrt{N_t}}[1,e^{j\pi\sin\theta},\dots,e^{j(N_t-1)\pi\sin\theta}]^T$  and  $\boldsymbol{a}_T(\phi) = \frac{1}{\sqrt{N_r}}[1,e^{j\pi\sin\phi},\dots,e^{j(N_r-1)\pi\sin\phi}]^T.$ 

Given the time-domain channel  $\mathbf{H}[d]$ , the corresponding frequency-domain channel at subcarrier-k can be obtained ass

$$H[k] = \sum_{d=0}^{N_c - 1} \mathbf{H}[d] e^{-j\frac{2\pi}{K}kd}.$$
 (2)

Let  $s[k] \in \mathbb{C}^{N_s \times 1}$  be the transmitted vector at subcarrier-k with  $E\{\|s[k]\|^2\} = 1$ . By taking the hybrid precoding into account, the received signal at subcarrier-k is expressed as

$$\boldsymbol{r}[k] = \boldsymbol{H}[k] \boldsymbol{U}_t \boldsymbol{P}[k] \boldsymbol{s}[k] + \boldsymbol{\omega}[k], \tag{3}$$

where  $P[k] \in \mathbb{C}^{N_s \times N_s}$  is the digital precoder at subcarrierk;  $U_t \in \mathbb{C}^{N_t \times N_s}$  is the shared RF precoder;  $\omega[k] \sim \mathcal{CN}(\mathbf{0}, \sigma^2 \mathbf{I}_{N_r})$  is the white Gaussian noise.

After being combined by  $U_r \in \mathbb{C}^{N_r \times N_s}$  in the RF domain, the received signal in digital baseband becomes

$$y[k] = U_{r}^{*}r[k] = U_{r}^{*}H[k]U_{t}P[k]s[k] + \eta[k], \quad (4)$$

where  $\eta[k] = U_r^* \omega[k]$ . Note that  $U_t$  and  $U_r$  are implemented in the time domain, which means that they are common for all subcarriers [9]. Additionally, since the analog part is implemented via the b-bit analog phase shifters (APSs), all entries of  $U_t$  are constant modulus; that is  $(U_t)_{i,j} = \frac{1}{\sqrt{N_t}} e^{j\phi_{i,j}}$  with  $\phi_{i,j} \in \mathbb{B} = \{0, \frac{2\pi}{2^b}, \dots, \frac{2\pi(2^b-1)}{2^b}\}$ . Similar is the case for  $U_r$ .

# III. HPSM DESIGN

As has been mentioned before, hPSM includes the digital part and the analog part. In this section, we elaborate on the details of these two parts.

 $\begin{array}{c} \text{TABLE I} \\ \text{BPSK Modulation With } \{N_s=2, N_a=1, \text{BPSK}\} \end{array}$ 

Input bits	RF chain status	Output symbol
[0, 0]	{ON, OFF}	(+1,0)
[0, 1]	{OFF, ON}	(0, +1)
[1, 0]	{ON, OFF}	(-1,0)
[1, 1]	{OFF, ON}	(0, -1)

#### A. The Digital Design

Denote  $\boldsymbol{H}_{ak} = \boldsymbol{U}_r \boldsymbol{H}[k] \boldsymbol{U}_t$  as the VSC at subcarrierk. To reduce the receiver complexity, Zero-Forcing (ZF) pre-equalizer is set as the digital precoder:

$$P[k] = \beta_k H_{ak}^* (H_{ak} H_{ak}^*)^{-1} = \beta_k P_n[k],$$
 (5)

where  $\beta_k = \sqrt{N_s \{tr[(\boldsymbol{U}_t \boldsymbol{P}_n[k])(\boldsymbol{U}_t \boldsymbol{P}_n[k])^*]\}^{-1}}$  is the power normalization factor. Then the received signal in Eq. (4) is given by

$$\boldsymbol{y}[k] = \beta_k \boldsymbol{s}[k] + \boldsymbol{\eta}[k]. \tag{6}$$

Based on VSC, hPSM maps the symbol bits into conventional modulated symbols chosen from the constellation diagram, and the index bits into activation status of the receive RF chains. A total of  $N_a < N_s$  RF chains can be activated to facilitate simultaneous transmission of  $N_a$  data streams. Here an example of hPSM using binary PSK (BPSK) is provided in Table I. With the similar mapping manner employed of all subcarriers, the spectral efficiency per subcarrier can be expressed as

$$k_{eff} = |\log_2 |\mathcal{C}_r|| + N_a k_{mod}, \tag{7}$$

where  $C_r$  contains all possible index patterns and  $k_{mod}$  is the order of the conventional modulation.

#### B. The Analog Design

At the first sight, one may think that hPSM is almost identical to PSM, whose design is accomplished once P[k] is determined. However, once taking a closer look at Eq. (5), one may find that the so-called digital part is essentially determined by the analog part ( $U_r$  and  $U_t$ ). More importantly,  $U_r$  and  $U_t$  remain the same at all subcarriers and await a further optimization. To this end, we then elaborate on how to determine the analog part of hPSM. Based on the criterion of minimizing error performance, the corresponding analog part optimization problem can be formulated as follows

P.1 
$$\underset{\boldsymbol{U}_r, \boldsymbol{U}_t}{\operatorname{arg \, min}} P_e(\boldsymbol{U}_r, \boldsymbol{U}_t)$$
  
 $s.t. \ \forall i, j \angle (\boldsymbol{U}_t)_{i,j} \in \mathbb{B}, \quad \forall m, n \angle (\boldsymbol{U}_r)_{m,n} \in \mathbb{B}.$  (8)

Apparently, solving P.1 requires an explicit expression of  $P_e$ . Considering the intractability of analyzing BER precisely, we first derive the APEP for further process.

*Proposition 1:* For a hybrid mmWave mMIMO system with *K* subcarriers, the APEP of hPSM via maximum-likelihood (ML) detection can be approximated as

$$P_e \approx \frac{\gamma}{K} \sum_{k=1}^{K} Q(\beta_k \cdot \lambda),$$
 (9)

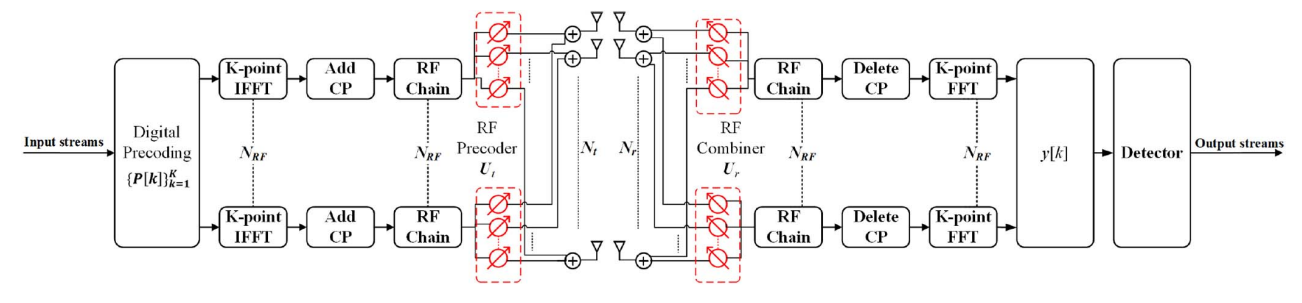


Fig. 1. A block diagram of the hybrid mmWave mMIMO system.

where  $\gamma$  is a constant determined by the mapping manner,  $\lambda$  is a fixed factor defined in the Appendix, and  $Q(\cdot)$  represents the Gaussian-Q function.

*Proof:* See the Appendix.

Although this is an explicit form of  $P_e$ , it is still intractable for getting the optimal solution to P.1 as the entry-wise constraints in Eq. (8) make P.1 an NP-hard problem. Hence it is necessary to shrink the search space. To this end, we aim at the design of proper codebooks, so that the entry-wise constraints can degenerate into column-wise constraints. For finite-resolution APS, the transmitter codebook  $\mathcal{F}_t$  can be expressed as

$$\mathcal{F}_t = \{\mathfrak{F}(\boldsymbol{a}_t(0)), \mathfrak{F}(\boldsymbol{a}_t(\Omega_1)), \dots, \mathfrak{F}(\boldsymbol{a}_t(\Omega_{N_t-1}))\}, \quad (10)$$
 where  $\Omega_n = \arcsin\frac{2n}{N_t}, 0 \leq n \leq N_t-1; \mathfrak{F}$  is the quantization function [10] defined as

$$\mathfrak{F}(\boldsymbol{a}_{t}(\Omega_{n})) = \underset{\alpha \in \mathcal{B}}{\operatorname{arg\,min}} \left\| \frac{1}{\sqrt{N_{t}}} e^{j\alpha} - (\boldsymbol{a}_{t}(\Omega_{n}))_{i} \right\|^{2},$$

$$\forall n \in [0, N_{t} - 1], \forall i \in [1, N_{t}]. \tag{11}$$

For ideal APSs, the quantization operation can be omitted. A similar process is applied to  $\mathcal{F}_r$ , thus being omitted here. As a consequence, the original P.1 is simplified into P.2 as follows:

P.2 
$$\underset{\boldsymbol{U}_r, \boldsymbol{U}_t}{\operatorname{arg\,min}} \sum_{k=1}^K Q(\beta_k \cdot \lambda)$$
  
s.t.  $\forall i \quad (\boldsymbol{U}_t)_{:,i} \in \mathcal{F}_t, \quad \forall j \quad (\boldsymbol{U}_r)_{:,j} \in \mathcal{F}_r.$  (12a)

Towards P.2, we propose an approach consisting of a greedy codebook search (GCS) and an entry update (EU) to construct  $U_t$  and  $U_r$ . Specifically, at each iteration, one codeword pair that can minimize  $P_e$  will be selected from  $\mathcal{F}_t$  and  $\mathcal{F}_r$ , respectively. The process keeps running until  $N_s$  codeword pairs are selected to construct  $U_t$  and  $U_r$ . After this, to further reduce  $P_e$ , one could further greedily update the entries of  $U_t$  and  $U_r$  in an alternating manner similar to [11].

#### IV. SIMULATIONS

In this section, numerical simulations are provided to evaluate the BER performance of hPSM in an mmWave mMIMO system with  $N_t=32$  and  $N_r=16$ . The channel related parameters are set as:  $N_p=8$ ; p(t) is the raised-cosine function with a roll-off factor R=0.8;  $N_c=4$ ,  $T_s=10^{-9}{\rm s}$  and

 $^1$ In practice, the alternating operation could be performed multiple times until reaching a certain terminating condition. While in the following simulations we only perform one-time alternation, i.e., greedily updating the entire  $U_T$  and  $U_t$  once, it suffices to validate the functionality of entry-wise update.

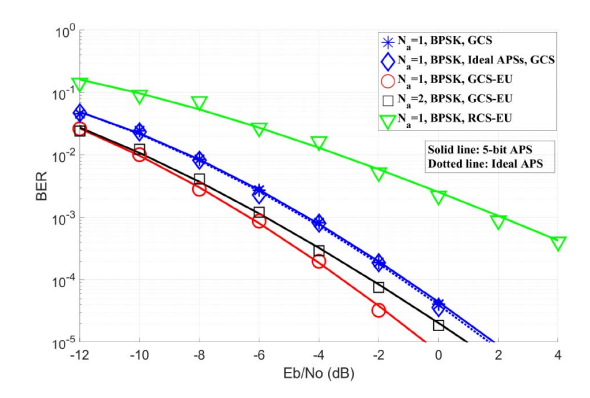


Fig. 2. BER comparisons among different VSC construction methods under  $\{N_s=2, N_a=1, \mathrm{BPSK}\}$ .

K=16. Without loss of generality, 5-bit APSs are adopted at the transceivers. For all figures, the signal-to-noise ratio (SNR) is defined as  $E_b/N_0=\frac{1}{k_{eff}\sigma^2}$ . All results are obtained by averaging of over 10000 independent channel realizations, with each having a block length of 2000.

To verify the importance of VSC in hPSM, in Fig. 2, we specifically compare the BER performance achieved by different VSC construction methods: GCS only, GCS with EU (GCS-EU), and random codebook search with EU (RCS-EU). The conventional steering with ideal APSs is set as the benchmark. The hPSM setup is  $\{N_s=2,N_a=1,\mathrm{BPSK}\}$ , with b=5. Fig. 2 shows that the performance of GCS is very similar to that of the steering method. Moreover, with the help of EU, the BER advantage of GCS-EU over GCS is 2 dB. For RCS-EU with two-stage processing, its performance is still largely inferior to others, indicating that the initial point may heavily influence the final performance. This is mainly due to the sub-optimality nature of the proposed method, and a superior optimization scheme will be left as the future work.

In Fig. 3 we compare the BER performance of hPSM and non-hPSM schemes under various  $k_{eff}$  values. For  $k_{eff}=2$  bits/s/Hz, the advantage of hPSM with  $\{N_s=2,N_a=2,N_a=1,\mathrm{BPSK}\}$  over non-hPSM with  $\{N_s=2,N_a=2,\mathrm{BPSK}\}$  is about 1.5 dB. When increasing  $k_{eff}$  from 2 to 4, hPSM with  $\{N_s=4,N_a=2,\mathrm{BPSK}\}$  outperforms non-hPSM with  $\{N_s=4,N_a=2,\mathrm{BPSK}\}$  by more than 1 dB. From Fig. 3(c), we further notice that hPSM with  $\{N_s=4,N_a=2,\mathrm{quadrature}\,\mathrm{PSK}(\mathrm{QPSK})\}$  and  $\{N_s=4,N_a=1,16\mathrm{-QAM}\}$  both outperform non-hPSM with  $\{N_s=4,N_a=4,\mathrm{BPSK}\}$ . This implies that hPSM could enjoy a higher spectral efficiency and a better error performance simultaneously.

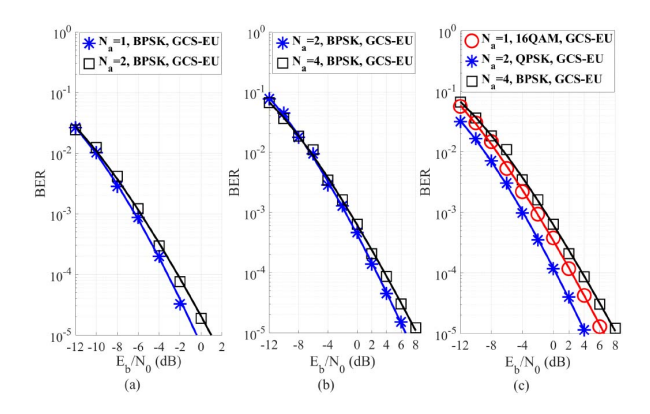


Fig. 3. BER comparisons under different  $k_{\it eff}$  values: (a)  $k_{\it eff}=2$  bits/s/Hz; (b)  $k_{\it eff}=4$  bits/s/Hz; (c)  $k_{\it eff}=6$  bits/s/Hz.

## V. CONCLUSION

In this letter, we have proposed a novel index modulation termed as hPSM for hybrid mmWave mMIMO systems over frequency-selective channels. The concept of hPSM originates from PSM, but is strikingly different. This is because hPSM is essentially a technique dependent upon the analog part which remains common for all subcarriers in hybrid mmWave mMIMO. By carefully designing the analog part based on the criterion of APEP minimization, the error performance of hPSM is optimized with low complexity and demonstrated to be advantageous over its non-hPSM counterpart.

### APPENDIX

Let  $s_m^i[k]$  denote that the activation status of RF chains is i and the conventional modulated symbol streams  $b_m$  is transmitted. With ML detector used at the transmitter, we have

$$\widehat{\boldsymbol{s}}[k] = \underset{\boldsymbol{s}_{m}^{i} \in \mathbb{S}}{\operatorname{arg\,min}} \|\boldsymbol{y}[k]/\beta_{k} - \boldsymbol{\eta}[k]\|^{2}, \tag{13}$$

where  $\mathbb{S}$  is the search space of the super-symbol  $s_m^i$ . The union-bound approach is adopted to derive APEP like [4], giving rise to

$$P_{ek} \leq \frac{1}{k_{eff}|\mathbb{S}|} \sum_{\substack{\boldsymbol{s}_{m}^{i} \in \mathbb{S} \\ \boldsymbol{s}_{m}^{j} \neq \boldsymbol{s}^{i}}} \sum_{\substack{\boldsymbol{s}_{n}^{j} \in \mathbb{S} \\ \boldsymbol{s}_{m}^{j} \neq \boldsymbol{s}^{i}}} d(\boldsymbol{s}_{m}^{i}, \boldsymbol{s}_{n}^{j}) P_{r}(\boldsymbol{s}_{m}^{i} \to \boldsymbol{s}_{n}^{j}), (14)$$

where  $P_r(s_m^i \to s_n^j)$  denotes the pairwise error probability;  $d(s_m^i, s_n^j)$  denotes the bit-type Hamming distance between  $s_m^i$  and  $s_n^j$ .

(i) Case 1 ( $N_a = 1$ ): When  $N_a = 1$ ,  $P_r(s_m^i \to s_n^j)$  can be classified into the following three cases

$$P_{r}(\boldsymbol{s}_{m}^{i} \rightarrow \boldsymbol{s}_{n}^{j}) = \begin{cases} P_{i}(\boldsymbol{s}_{m}^{i} \rightarrow \boldsymbol{s}_{m}^{j}), & \text{if } i \neq j, m = n \\ P_{m}(\boldsymbol{s}_{m}^{i} \rightarrow \boldsymbol{s}_{n}^{i}), & \text{if } i = j, m \neq n \\ P_{mi}(\boldsymbol{s}_{m}^{i} \rightarrow \boldsymbol{s}_{n}^{j}), & \text{if } i \neq j, m \neq n, \end{cases}$$
(15)

where 
$$P_i(\boldsymbol{s}_m^i \to \boldsymbol{s}_m^j) = Q(\beta_k \cdot \frac{|b_m|}{\sqrt{N_0}}), \ P_m(\boldsymbol{s}_m^i \to \boldsymbol{s}_n^i) = Q(\beta_k \cdot \frac{|b_m-b_n|}{\sqrt{2N_0}}) \text{ and } P_{mi}(\boldsymbol{s}_m^i \to \boldsymbol{s}_n^i) = Q(\beta_k \cdot \sqrt{\frac{|b_m|^2 + |b_n|^2}{2N_0}}).$$
Let  $\lambda = \min\{\frac{|b_m|}{\sqrt{N_0}}, \frac{|b_m-b_n|}{\sqrt{2N_0}}, \sqrt{\frac{|b_m|^2 + |b_n|^2}{2N_0}}\}$ , then
$$P_r(\boldsymbol{s}_m^i \to \boldsymbol{s}_n^i) \leq Q(\beta_k \cdot \lambda). \tag{16}$$

(ii) Case 2 ( $N_a \ge 2$ ): For  $N_a \ge 2$ ,  $P_r(s_m^i \to s_n^j)$  can be expressed as

$$P(\boldsymbol{s}_{m}^{i} \to \boldsymbol{s}_{n}^{j}) = Q\left(\beta_{k} \cdot \sqrt{\frac{A+B}{N_{0}}}\right),$$
 (17)

where  $A=\sum_{r\in\Psi_0}\frac{|b_{n_r}|^2+|b_{m_r}|^2}{2}$  and  $B=\sum_{r\in\Psi_1}\frac{|b_{n_r}-b_{m_r}|^2}{2}$ .  $\Psi_1$  denotes the set of indices that are correctly detected and  $\Psi_0$  denotes the complementary set of  $\Psi_1$ .

Let 
$$\lambda = \min\{\sqrt{\frac{A+B}{N_0}}\}$$
, then

$$P_r(\boldsymbol{s}_m^i \to \boldsymbol{s}_n^j) \le Q(\beta_k \cdot \lambda). \tag{18}$$

(19)

Eqs. (16) and (18) tell that the pairwise error probability could be unified as

$$P_{ek} \leq \frac{1}{k_{eff}|\mathbb{S}|} \sum_{\substack{\boldsymbol{s}_{m}^{i} \in \mathbb{S} \\ \boldsymbol{s}_{n}^{j} \neq \boldsymbol{s}_{m}^{i}}} \sum_{\substack{\boldsymbol{s}_{m}^{i} \in \mathbb{S} \\ \boldsymbol{s}_{m}^{i} \neq \boldsymbol{s}_{m}^{i}}} d(\boldsymbol{s}_{m}^{i}, \boldsymbol{s}_{n}^{j}) Q(\beta_{k} \cdot \lambda) = \gamma_{k} Q(\beta_{k} \cdot \lambda),$$

with  $\gamma_k = \frac{1}{k_{eff}|\mathbb{S}|} \sum_{\boldsymbol{s}_m^i \in \mathbb{S}} \sum_{\boldsymbol{s}_n^j \in \mathbb{S}} s_n^j \neq \boldsymbol{s}_m^i d(\mathbf{s}_m^i, \mathbf{s}_n^j)$  dependent on the mapping manner of subcarrier-k only.

Combining  $N_a=1$  and  $N_a\geq 2$ , with the same mapping manner employed of all subcarriers, i.e.,  $\gamma_1=\gamma_2=\ldots=\gamma_K=\gamma$ , a general system APEP can be finally approximated as

$$P_e = \frac{1}{K} \sum_{k=1}^K P_{ek} \approx \frac{1}{K} \sum_{k=1}^K \gamma_k \cdot Q(\beta_k \cdot \lambda) = \frac{\gamma}{K} \sum_{k=1}^K Q(\beta_k \cdot \lambda).$$
(20)

# REFERENCES

- [1] R. Y. Mesleh, H. Haas, S. Sinanovic, C. W. Ahn, and S. Yun, "Spatial modulation," *IEEE Trans. Veh. Technol.*, vol. 57, no. 4, pp. 2228–2241, Jul. 2008.
- [2] X. Cheng, M. Zhang, M. Wen, and L. Yang, "Index modulation for 5G: Striving to do more with less," *IEEE Wireless Commun.*, vol. 25, no. 2, pp. 126–132, Apr. 2018.
- [3] A. Younis, N. Serafimovski, R. Mesleh, and H. Haas, "Generalised spatial modulation," in *Proc. Conf. Rec. 44th Asilomar Conf. Signals Syst. Comput.*, Pacific Grove, CA, USA, 2010, pp. 1498–1502.
- [4] R. Zhang, L.-L. Yang, and L. Hanzo, "Generalised pre-coding aided spatial modulation," *IEEE Trans. Wireless Commun.*, vol. 12, no. 11, pp. 5434–5443, Nov. 2013.
- [5] J. Li, M. Wen, M. Zhang, and X. Cheng, "Virtual spatial modulation," IEEE Access, vol. 4, pp. 6929–6938, 2016.
- [6] O. E. Ayach, S. Rajagopal, S. Abu-Surra, Z. Pi, and R. W. Heath, "Spatially Sparse Precoding in Millimeter Wave MIMO Systems," *IEEE Trans. Wireless Commun.*, vol. 13, no. 3, pp. 1499–1513, Mar. 2014.
- [7] S. Gao, X. Cheng, and L. Yang, "Spatial multiplexing with limited RF chains: Generalized beamspace modulation (GBM) for mmWave massive MIMO," *IEEE J. Sel. Areas Commun.*, vol. 37, no. 9, pp. 2029–2039, Sep. 2019.
- [8] E. Başar, Ü. Aygölü, E. Panayirci, and H. V. Poor, "Orthogonal frequency division multiplexing with index modulation," *IEEE Trans. Signal Process.*, vol. 61, no. 22, pp. 5536–5549, Nov. 2013.
- [9] A. Alkhateeb and R. W. Heath, "Frequency selective hybrid precoding for limited feedback millimeter wave systems," *IEEE Trans. Commun.*, vol. 64, no. 5, pp. 1801–1818, May 2016.
- [10] J. Mao, Z. Gao, Y. Wu, and M. Alouini, "Over-sampling codebook-based hybrid minimum sum-mean-square-error precoding for millimeter-wave 3D-MIMO," *IEEE Wireless Commun. Lett.*, vol. 7, no. 6, pp. 938–941, Dec. 2018.
- [11] C. Chen, "An iterative hybrid transceiver design algorithm for millimeter wave MIMO systems," *IEEE Wireless Commun. Lett.*, vol. 4, no. 3, pp. 285–288, Jun. 2015.